Article

Neuron

Age-Dependent Specific Changes in Area CA2 of the Hippocampus and Social Memory Deficit in a Mouse Model of the 22q11.2 Deletion Syndrome

Highlights

- The 22q11.2 deletion mouse model displays unique changes in hippocampal area CA2
- There is an age-dependent reduction in PV+ interneurons and inhibitory transmission
- Inhibitory transmission is less plastic, and pyramidal cells in CA2 are less excitable
- Social memory is strongly impaired in the 22q11.2 deletion mouse model

Authors

Rebecca A. Piskorowski, Kaoutsar Nasrallah, Anastasia Diamantopoulou, ..., Steven A. Siegelbaum, Joseph A. Gogos, Vivien Chevaleyre

Correspondence

jag90@cumc.columbia.edu (J.A.G.), vivien.chevaleyre@parisdescartes.fr (V.C.)

In Brief

In a mouse model of the 22q11.2 deletion syndrome, Piskorowski et al. reveal the consequences of a loss of inhibition in hippocampal area CA2 during early adulthood, revealing a mechanism potentially underlying social cognitive dysfunction in psychiatric diseases including schizophrenia.

Piskorowski et al., 2016, Neuron *89*, 163–176
January 6, 2016
http://dx.doi.org/10.1016/j.neuron.2015.11.036

CellPress

Neuron
Article

Age-Dependent Specific Changes in Area CA2 of the Hippocampus and Social Memory Deficit in a Mouse Model of the 22q11.2 Deletion Syndrome

Rebecca A. Piskorowski,[1] Kaoutsar Nasrallah,[1] Anastasia Diamantopoulou,[2,3] Jun Mukai,[3] Sami I. Hassan,[4,5] Steven A. Siegelbaum,[4,5] Joseph A. Gogos,[3,4,*] and Vivien Chevaleyre[1,*]
[1]CNRS UMR8118, Team Synaptic Plasticity and Neural Networks, Université Paris Descartes, 75006 Paris, France
[2]Department of Psychiatry
[3]Department of Physiology and Cellular Biophysics
[4]Department of Neuroscience
[5]Department of Pharmacology
College of Physicians and Surgeons, Columbia University, New York, NY 10032, USA
*Correspondence: jag90@cumc.columbia.edu (J.A.G.), vivien.chevaleyre@parisdescartes.fr (V.C.)
http://dx.doi.org/10.1016/j.neuron.2015.11.036

SUMMARY

Several neuropsychiatric disorders are associated with cognitive and social dysfunction. Postmortem studies of patients with schizophrenia have revealed specific changes in area CA2, a long-overlooked region of the hippocampus recently found to be critical for social memory formation. To examine how area CA2 is altered in psychiatric illness, we used the *Df(16)A*$^{+/-}$ mouse model of the 22q11.2 microdeletion, a genetic risk factor for developing several neuropsychiatric disorders, including schizophrenia. We report several age-dependent CA2 alterations: a decrease in the density of parvalbumin-expressing interneurons, a reduction in the amount of feedforward inhibition, and a change in CA2 pyramidal-neuron intrinsic properties. Furthermore, we found that area CA2 is less plastic in *Df(16)A*$^{+/-}$ mice, making it nearly impossible to evoke action potential firing in CA2 pyramidal neurons. Finally, we show that *Df(16)A*$^{+/-}$ mice display impaired social cognition, providing a potential mechanism and a neural substrate for this impairment in psychiatric disorders.

INTRODUCTION

While much recent progress has been made in understanding the genetic causes of psychiatric illnesses, there remain many unresolved questions pertaining to the neural substrates at the cellular and circuitry levels underlying specific symptoms and cognitive deficits. One area in particular that merits further study is the long-overlooked area CA2 of the hippocampus. It was shown recently that area CA2 is critical for social memory formation (Hitti and Siegelbaum, 2014; Stevenson and Caldwell, 2014), likely plays little role in spatial coding (Lee et al., 2015; Lu et al., 2015; Mankin et al., 2015), and may serve to detect conflicts between memory-driven and sensory information converging on the hippocampus (Wintzer et al., 2014). Before the contribution of area CA2 to hippocampal function was appreciated, numerous postmortem studies of schizophrenic and psychotic patients had revealed that this relatively small hippocampal region undergoes disease-related changes in size and composition (Benes et al., 1998; Narr et al., 2004). A meta-analysis study reported that a decrease in parvalbumin-expressing (PV+) interneuron (IN) density in area CA2 was one of the few measures, of more than 200, to be significantly altered in schizophrenia and bipolar disorder in the hippocampus (Knable et al., 2004). A decrease in PV+ INs in CA2 has also been reported in Alzheimer's disease (Brady and Mufson, 1997). Therefore, understanding cellular alterations that occur in area CA2 in psychiatric disorders is likely to provide invaluable information about the pathogenesis of these diseases. To this end, we analyzed CA2 in a mouse model of the 22q11.2 deletion syndrome (22q11.2DS), as this allows a more reliable and comprehensive examination of the consequences of the disease on cellular function and circuitry dynamics.

Individuals with the 22q11.2 deletion are sometimes given other diagnoses early in life, including attention-deficit hyperactivity disorder, generalized anxiety disorder, obsessive-compulsive disorder, and autism spectrum disorders (ASDs) (Karayiorgou et al., 2010). In late adolescence and early adulthood, up to one-third of all individuals carrying the 22q11.2 deletion develop schizophrenia or schizoaffective disorder, an approximately 30-fold increase in disease risk. Moreover, de novo 22q11.2 deletions account for up to 1%–2% of sporadic schizophrenia cases (International Schizophrenia Consortium, 2008; Karayiorgou et al., 1995; Xu et al., 2008). Most affected individuals carry a 3 Mb hemizygous deletion, whereas 7% have a nested 1.5 Mb deletion spanning 27 known genes (Karayiorgou et al., 2010). A mouse model, *Df(16)A*$^{+/-}$ mice (Stark et al., 2008), carrying an engineered orthologous deletion on mouse chromosome 16 encompassing all but one of the genes encoded in the 22q11.2 critical region, is a particularly powerful tool for deciphering how this genetic lesion increases risk for

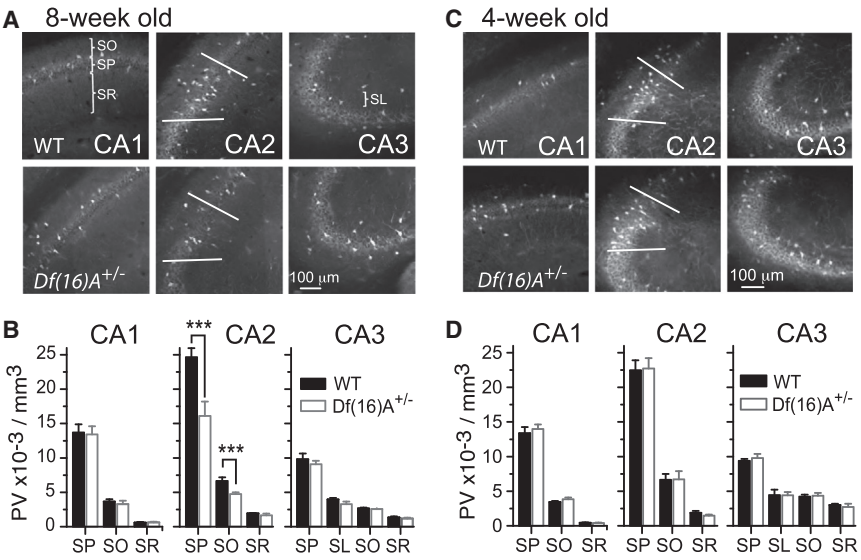

Figure 1. The Density of Parvalbumin-Expressing INs in the Hippocampus Is Decreased in Area CA2 of Adult *Df(16)A*$^{+/-}$ Mice

(A) Immunohistochemical staining for parvalbumin in the different hippocampal areas of the hippocampus from an 8-week-old WT and *Df(16)A*$^{+/-}$ mouse. The different hippocampal layers are indicated (*stratum oriens*, SO; *stratum pyramidale*, SP; *stratum radiatum*, SR; *stratum lucidum*, SL).

(B) Quantification of the density of parvalbumin-positive soma (PV+) in the different strata of areas CA1, CA2, and CA3 of 8-week-old WT and *Df(16)A*$^{+/-}$ mice (n = 6 mice for both genotypes).

(C) Immunohistochemical staining for parvalbumin in the different hippocampal areas of the hippocampus from a 4-week-old WT and *Df(16)A*$^{+/-}$ mouse.

(D) Quantification of the density of PV+ soma in the different strata of CA1, CA2, and CA3 areas in 4-week-old WT (n = 6) and *Df(16)A*$^{+/-}$ mice (n = 6). Error bars show SEM. See also Figure S1.

neuropsychiatric disorders. *Df(16)A*$^{+/-}$ mice have deficits in sensorimotor gating, emotional learning (Stark et al., 2008), and altered performance and long-range synchrony between the hippocampus and prefrontal cortex during a spatial working-memory task (Sigurdsson et al., 2010; Stark et al., 2008). However, besides the impairment in long-range connectivity between brain structures, the local cellular changes at the level of the hippocampal microcircuit are subtle in area CA1 (Drew et al., 2011; Earls et al., 2010) and completely unknown in areas CA2 and CA3. Given the reported alterations in area CA2 in patients with schizophrenia and other neuropsychiatric disorders, we decided to examine area CA2 of *Df(16)A*$^{+/-}$ mice and, in particular, the inhibitory transmission and activity-dependent plasticity mediated by PV+ INs.

We found that the density of PV+ INs in the hippocampus of *Df(16)A*$^{+/-}$ mice is specifically reduced in area CA2. Accompanying this reduction is an impairment of feedforward inhibition onto CA2 PNs and a larger excitatory drive from CA3 inputs. These effects are only observed after maturity to adulthood, paralleling the disease onset in humans. The intrinsic properties of CA2 PNs are also affected, resulting in a decreased action potential firing in response to proximal and distal excitatory input stimulation. The *Df(16)A*$^{+/-}$ mice display social memory impairment similar to that observed following specific silencing of CA2 PNs. These results show that the specific alterations reported in hippocampal CA2 in humans with schizophrenia are also present in *Df(16)A*$^{+/-}$ mice and may underlie impaired social cognition in this disorder.

RESULTS

The Density of PV+ INs in the Hippocampus Is Decreased Specifically in Area CA2 of Adult *Df(16)A*$^{+/-}$ Mice

In the hippocampus, both individual and meta-analysis of postmortem studies of individuals with schizophrenia have reported a significant decrease in PV+ IN density specifically in area CA2 (Benes et al., 1998; Berretta et al., 2009; Knable et al., 2004; Zhang and Reynolds, 2002). Therefore, we first asked whether a similar change in PV+ IN density occurred in area CA2 of *Df(16)A*$^{+/-}$ mice. To this end, we performed immunostaining against PV and quantified the density of PV+ cells in the different subdivisions of the hippocampus in adult mice (8 weeks old). Consistent with previous findings (Botcher et al., 2014; Piskorowski and Chevaleyre, 2013), the density of PV+ INs in wild-type littermate control mice (WT) was higher in area CA2 *stratum oriens* (SO) and *stratum pyramidale* (SP) than in the other hippocampal areas (Figures 1A and 1B). In *Df(16)A*$^{+/-}$ mice, the density of PV+ INs in area CA2 was significantly lower than in WT mice (results for SO were as follows: 6,650 ± 525 for WT versus 4,691 ± 239 for *Df(16)A*$^{+/-}$ mice, p = 0.0068; results for SP were as follows: 24,664 ± 1,307 for WT versus 16,110 ± 2,071 for *Df(16)A*$^{+/-}$ mice, p = 0.0058; n = 6 mice for both WT and *Df(16)A*$^{+/-}$ mice). Strikingly, this decrease in PV+ cell density was specific to area CA2, as no changes were observed in areas CA1 and CA3 (Figure 1B). To ensure that the quantification of PV+ density in CA2 was not biased by a change in the size of area CA2 in *Df(16)A*$^{+/-}$ mice, we also performed costaining with the CA2-specific marker regulator of G protein signaling 14 (RGS14) (Lee et al., 2010). We found no difference between WT and *Df(16)A*$^{+/-}$ mice in the area of the hippocampus stained by the RGS14 antibody, indicating that the size of area CA2 is unchanged. Moreover, with the boundaries between the CA areas defined by RGS14 staining alone, we confirmed the significant decrease in the density of PV+ cells in CA2 area of *Df(16)A*$^{+/-}$ mice (Figure S1, available online; SP results were as follows: p = 0.008; n = 3 and 4 mice for WT and *Df(16)A*$^{+/-}$ mice, respectively).

The typical onset of behavioral symptoms of schizophrenia occurs during early adulthood. We wondered whether the change we observed in PV+ IN density might also be age dependent. Therefore, we quantified the density of PV+ INs in 4-week-old mice. The density of PV+ cells in 4-week-old WT mice was similar to that observed in older mice. Notably, however, the density of PV+ cells in area CA2 was identical between

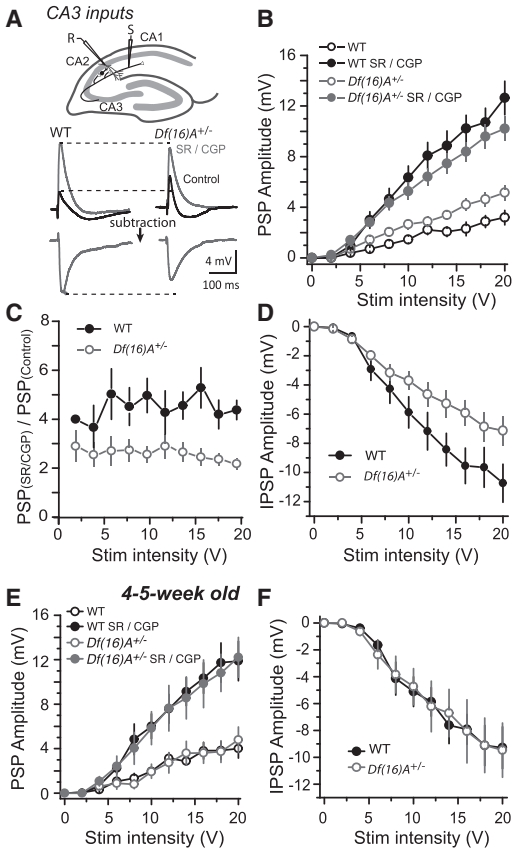

Figure 2. Inhibitory Transmission onto CA2 PNs Is Decreased in Adult *Df(16)A*$^{+/-}$ Mice

(A) Top: schematic representation of the experimental conditions in which a compound EPSP/IPSP sequence was recorded in CA2 pyramidal neurons (PNs) following stimulation of Schaffer collaterals (SC). Middle: sample traces of the compound EPSP/IPSP (control, black traces) and the EPSP obtained after blocking inhibition (SR/CGP, gray traces) in CA2 PNs in response to stimulation of SC inputs in WT and *Df(16)A*$^{+/-}$ mice. Bottom: the inhibitory component obtained after subtracting the control traces from the traces with GABA receptor blockers is shown in gray.

(B) Summary graph of the input-output curves of the PSP in control conditions and after blocking inhibition (SR/CGP) in response to SC stimulation in adult WT (n = 8) and *Df(16)A*$^{+/-}$ mice (n = 17).

(C) Summary graph of the fold-increase in PSP amplitude after blocking inhibition in WT and *Df(16)A*$^{+/-}$ mice.

(D) Summary graph of the input-output curves of the IPSP amplitude obtained by subtraction of control traces from the traces with GABA receptor blockers in WT and in *Df(16)A*$^{+/-}$ mice.

(E) Summary graph of the input-output curves of the PSPs in response to SC stimulation in control conditions and following blockade of inhibitory transmission in young (4- to 5-week-old) WT (n = 6) and *Df(16)A*$^{+/-}$ mice (n = 5).

(F) Summary graph of the input-output curves of the IPSP in response to CA3 input stimulation obtained by subtracting control traces from traces with GABA receptor blockers in 4- to 5-week-old WT and *Df(16)A*$^{+/-}$ mice. Error bars show SEM. See also Figure S2.

WT and *Df(16)A*$^{+/-}$ mice (Figures 1C and 1D; SO results were as follows: 6,662 ± 839 for WT versus 6,703 ± 1,203 for *Df(16)A*$^{+/-}$ mice, p = 0.97; SP results were as follows: 22,430 ± 1,465 for WT versus 22,728 ± 1,496 for *Df(16)A*$^{+/-}$ mice, p = 0.89; n = 6 for WT and 6 for *Df(16)A*$^{+/-}$ mice). Overall, our results show that the *Df(16)A*$^{+/-}$ mice recapitulate one of the most consistent cellular phenotypes observed in the hippocampus of patients with schizophrenia, i.e., an age-dependent decrease in PV+ cell density in area CA2.

The Inhibitory Control of Excitatory Drive from CA3 Is Reduced in Adult *Df(16)A*$^{+/-}$ Mice

Inhibitory transmission in area CA2 powerfully controls the strength of excitatory transmission from the Schaeffer collateral (SC) inputs and completely prevents CA3 neurons from evoking action potential firing in CA2 pyramidal neurons (PNs). To address whether the decrease in PV+ neurons observed in *Df(16)A*$^{+/-}$ mice could affect the control of the excitatory drive from CA3 PNs, we monitored the postsynaptic potentials (PSPs) in CA2 PNs in response to stimulation of SC inputs before and after blockade of GABA receptors. The depolarizing phase of the PSP in control conditions was very small in WT mice and was truncated by a large hyperpolarizing component. The addition of GABA receptor blockers markedly increased the amplitude of the excitatory PSP (EPSP; Figures 2A and 2B). In the absence of GABA receptor blockers, the depolarizing component of the PSP was significantly larger in *Df(16)A*$^{+/-}$ mice than in WT mice (Figure 2B; n = 8, 3 mice for WT; n = 17, 6 mice for *Df(16)A*$^{+/-}$ mice; ANOVA two-way RM results for genotype were as follows: F(1,7) = 6.89, p = 0.03; results for stimulation were as follows: F(2.06,14.4) = 50.3, p = 0.00000027; and results for genotype × stimulation were as follows: F(2.6,18.4) = 2.03, p = 0.14).

However, in the presence of GABA receptor blockers, the EPSPs in WT and *Df(16)A*$^{+/-}$ mice were not different (Figures 2A and 2B; n = 8, 3 mice for WT; n = 17, 6 mice for *Df(16)A*$^{+/-}$ mice; ANOVA two-way RM results for genotype were as follows: F(1,6) = 0.00032, p = 0.98; results for stimulation were as follows: F(1.7,10.24) = 185.9, p = 1.37 × 10^{-8}; and results for genotype × stimulation were as follows: F(1.42,8.56) = 0.23, p = 0.72). When we examined the change in PSP amplitude before and after blocking inhibition, the 4- to 5-fold increase observed in WT mice was significantly reduced to 2- to 3-fold in *Df(16)A*$^{+/-}$ mice (Figure 2C; n = 8, 3 mice for WT; n = 17, 6 mice for *Df(16)A*$^{+/-}$ mice; ANOVA two-way RM results for genotype were as follows: F(1,7) = 6.89, p = 0.03; results for stimulation were as follows: F(2.1,14.4) = 50.3, p = 2.7 × 10^{-7}; and results for genotype × stimulation were as follows: F(2.6,18.4) = 2.03, p = 0.14). Finally, to isolate the inhibitory component evoked during the stimulation, we subtracted the responses in the presence of GABA receptor blockers from the responses with intact inhibition. Inferring the inhibitory PSP (IPSP) size from a compound EPSP-IPSP has previously been validated in other studies (Basu et al., 2013; Pouille and Scanziani, 2001). We found that the deduced IPSP was significantly smaller in *Df(16)A*$^{+/-}$ mice (Figure 2D; n = 8, 3 mice for WT; n = 17, 6 mice for *Df(16)A*$^{+/-}$ mice; ANOVA two-way RM results for genotype were as follows: F(1,7) = 7.19, p = 0.03; results for stimulation were as follows: F(2.6,18.2) = 169.4, p = 3.7 × 10^{-13}; and results for genotype × stimulation were as follows: F(1.99,13.97) = 7.0, p = 0.0078). These results show that the depolarizing component of the compound EPSP-IPSP is larger in *Df(16)A*$^{+/-}$ mice and that this increased PSP in the absence of GABA receptor blockers results from a decrease in the level of inhibitory transmission.

Because the change in PV+ IN density is age dependent, we measured the amplitude of the PSPs with and without inhibition and quantified the amplitude of deduced IPSPs for 4- to 5-week-old mice. We observed no difference in the amplitude of the PSP between WT and *Df(16)A*$^{+/-}$ mice (Figure 2E; n = 6, 4 mice for WT; n = 5, 5 mice for *Df(16)A*$^{+/-}$ mice; ANOVA two-way RM results for genotype were as follows: F(1,4) = 1.38 × 10^{-7}, p = 0.99; results for stimulation were as follows: F(3.0,12.0) = 57.3, p = 2.14 × 10^{-7}; and results for genotype × stimulation were as follows: F(1.3,5.21) = 0.39, p = 0.61 for the PSP before blockers; ANOVA two-way RM results for genotype were as follows: F(1,3) = 0.12, p = 0.74; results for stimulation were as follows: F(1.9,5.8) = 148.2, p = 1.08 × 10^{-5}; and results for genotype × stimulation were as follows: F(1.3,3.9) = 0.25, p = 0.70 after GABA blockers). We also observed no difference in the amplitude of the deduced IPSP (Figure 2F; n = 6, 4 mice for WT; n = 5, 5 mice for *Df(16)A*$^{+/-}$ mice; ANOVA two-way RM results for genotype were as follows: F(1,3) = 0.036, p = 0.86; results for stimulation were as follows: F(1.7,5.17) = 66.5, p = 2.3 × 10^{-4}; and results for genotype × stimulation were as follows: F(1.6,4.9) = 0.22, p = 0.76). Therefore, these results indicate that the decrease in PV+ IN number and in recruited inhibition results from of a change during periadolescent development.

The inhibition onto pyramidal cells comes from the recruitment of feedforward inhibition engaged by the SC but also potentially from a direct activation of inhibitory cells and axons by the stimulating electrode. To address whether the feedforward inhibition is impaired in *Df(16)A*$^{+/-}$ mice, we directly monitored inhibitory postsynaptic currents (IPSCs) at a holding potential of 0 mV (the reversal potential for excitatory currents) before and after blocking excitatory transmission. In control conditions, both the directly activated inhibition and the feedforward inhibition will be present, while only directly activated inhibition will be monitored after blocking excitation. We quantified the amount of feedforward inhibition by subtracting IPSCs in AMPA/NMDA blockers from the IPSCs in control conditions. We found that the level of feedforward inhibition was ~30% larger in WT mice compared to *Df(16)A*$^{+/-}$ mice (Figures S2A and S2B; for instance, at 20V stimulation the results for WT were as follows: 1,764.8 ± 262.1 pA, n = 17, 7 mice; and the results for *Df(16)A*$^{+/-}$ mice were as follows: 1,274.1 ± 211.9 pA, n = 15, 7 mice; ANOVA two-way RM results for genotype were as follows: F(1,13) = 5.59, p = 0.034; results for stimulation were as follows: F(1.6,21.0) = 51.47, p = 2.79 × 10^{-8}; and results for genotype × stimulation were as follows: F(1.96,25.5) = 0.95, p = 0.39).

The decrease in the level of feedforward inhibition could result from a decrease in the number of recruited INs or from a decrease in GABA release probability. We performed a paired stimulation to quantify the paired-pulse ratio (PPR) of two consecutive IPSCs, a parameter inversely proportional to release probability. When IPSCs were isolated in the presence of AMPA/NMDA receptor blockers, we found that the PPR (with a stimulation interval of 100 ms) was identical for WT and *Df(16)A*$^{+/-}$ mice over the entire stimulation intensity range (Figure S2C; n = 15, 6 mice for WT; n = 15, 6 mice for *Df(16)A*$^{+/-}$ mice; ANOVA two-way RM results for genotype were as follows: F(1,6) = 2.25, p = 0.18; results for stimulation were as follows: F(3.6,21.9) = 1.34, p = 0.28; and results for genotype × stimulation were as follows: F(2.3,14.2) = 0.70, p = 0.53). We also measured the PPR at different stimulation intervals (between 20 and 800 ms) and again found no difference between WT and *Df(16)A*$^{+/-}$ mice (Figure S2D; n = 10, 5 mice for WT; n = 11, 5 mice for *Df(16)A*$^{+/-}$ mice; ANOVA two-way RM results for genotype were as follows: F(1,8) = 0.27, p = 0.61; results for stimulation were as follows: F(2.2,17.9) = 4.4, p = 0.02; and results for genotype × stimulation were as follows: F(2.3,18.7) = 1.7, p = 0.20). Finally, because an increase in summation of synaptic responses during a train at CA3-CA1 excitatory synapses had previously been reported in *Df(16)A*$^{+/-}$ mice (Earls et al., 2010), we looked at the EPSP summation during a train of five pulses at the CA3-CA2 synapse. We found no difference between WT and *Df(16)A*$^{+/-}$ mice (Figure S2E; n = 6, 3 mice for WT; n = 7, 4 mice for *Df(16)A*$^{+/-}$ mice; ANOVA two-way RM results for genotype were as follows: F(1,3) = 0.10 p = 0.77; results for stimulation were as follows: F(1.8,5.6) = 102.6, p = 3.6 × 10^{-5}; and results for genotype × stimulation were as follows: F(1.2,3.6) = 0.15, p = 0.76). These results suggest that release probability at inhibitory synapses is not significantly altered in *Df(16)A*$^{+/-}$ mice and that the decrease in feedforward inhibition is likely a consequence of the decrease in PV+ IN function.

Distal Excitatory Transmission Is Not Affected in *Df(16)A*$^{+/-}$ Mice

CA2 PNs receive excitatory input from CA3 SCs on proximal apical dendrites and excitatory input from the entorhinal cortex on distal apical dendrites. To address whether the change we observed in *Df(16)A*$^{+/-}$ mice on the inhibitory control of excitatory transmission is input specific or a general feature in these mice, we stimulated in *stratum lacunosum moleculare* (SLM) and recorded PSPs before and after blocking inhibitory transmission. As reported previously, EPSPs from distal inputs were much less affected by blockade of inhibition than EPSPs from proximal inputs (Chevaleyre and Siegelbaum, 2010). We observed no difference in the PSP amplitude between adult WT and *Df(16)A*$^{+/-}$ mice, both in control conditions and following inhibition block (Figures 3A and 3B; n = 7, 3 mice for WT; n = 17, 6 mice for *Df(16)A*$^{+/-}$ mice; ANOVA two-way RM results for genotype were as follows: F(1,5) = 0.07, p = 0.79; results for stimulation were as follows: F(1.7,8.5) = 51.5, p = 2.25 × 10^{-5}; and results for genotype × stimulation were as follows: F(1.7,8.8) = 0.15, p = 0.83 before GABA receptor blockers; ANOVA two-way RM results for genotype were as follows: F(1,5) = 0.0018, p = 0.96; results for stimulation were as follows: F(1.6,8.0) = 101.05, p = 3.04 × 10^{-6}; and results for genotype × stimulation were as follows: F(1.7,8.7) = 0.52, p = 0.58 after GABA receptor blockers). Similarly, the increase in PSP amplitude after blocking inhibition and the deducted IPSP responses with and without GABA receptor blockers were also unaffected in *Df(16)A*$^{+/-}$ mice (Figures 3C and 3D; n = 7, 3 mice for WT; n = 17, 6 mice for *Df(16)A*$^{+/-}$ mice; ANOVA two- way RM results for genotype were as follows: F(1,2) = 0.019, p = 0.90; results for stimulation were as follows: F(1.2,2.4) = 4.07, p = 0.16; results for genotype × stimulation were as follows: F(1.7,3.4) = 0.039, p = 0.94 for the fold increase in PSP; ANOVA two-way RM results for genotype were as follows: F(1,5) = 0.31, p = 0.59; results

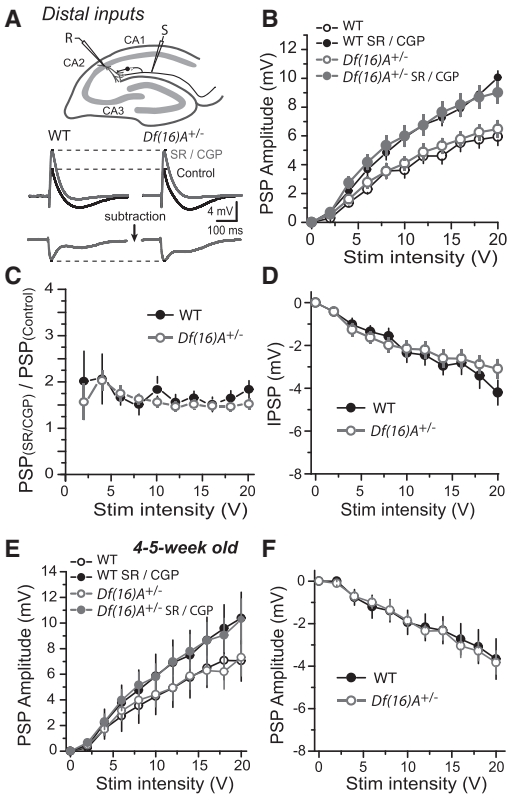

Figure 3. Synaptic Transmission of Distal Inputs onto CA2 PNs Is Not Altered in Adult *Df(16)A*$^{+/-}$ Mice

(A) Top: schematic representation of the experimental conditions in which a compound EPSP/IPSP sequence was recorded in CA2 PNs following stimulation of distal inputs. Bottom: sample traces of the compound EPSP/IPSP (control, black trace) and the EPSP obtained after blocking inhibition (SR/CGP, gray trace) in CA2 PNs in response to stimulation of distal inputs in WT and *Df(16)A*$^{+/-}$ mice. The inhibitory component obtained after subtracting the control traces from the traces with GABA receptor blockers is shown in gray.

(B) Summary graph of the input-output curves of the PSP amplitude in response to distal input stimulation in control conditions and after blocking inhibition in adult WT (n = 7) and *Df(16)A*$^{+/-}$ mice (n = 17).

(C) Summary graph of the fold increase in PSP amplitude after blocking inhibition in WT and *Df(16)A*$^{+/-}$ mice.

(D) Summary graph of the input-output curves of the IPSP obtained after subtraction of the control traces from traces with GABA receptor blockers in WT and in *Df(16)A*$^{+/-}$ mice.

(E) Summary graph of the input-output curves of PSPs in response to distal input stimulation in control conditions and after blocking inhibitory transmission in 4- to 5-week-old WT (n = 6) and *Df(16)A*$^{+/-}$ mice (n = 6).

(F) Summary graph of the input-output curves of the IPSP in response to distal input stimulation obtained by subtracting control traces from traces with GABA receptor blockers in 4- to 5-week-old WT and *Df(16)A*$^{+/-}$ mice. Error bars show SEM.

for stimulation were as follows: F(1.9,9.9) = 22.3, p = 226 × 10^{-4}; and results for genotype × stimulation were as follows: F(2.9,14.5) = 0.37, p = 0.76 for the IPSP).

We quantified the amplitude of the PSPs with and without inhibition and the amplitude of the deduced IPSPs in 4- to 5-week-old mice. We observed no difference in the amplitude of the PSP between WT and *Df(16)A*$^{+/-}$ mice (Figure 3E; n = 6, 3 mice for WT; n = 6, 4 mice for *Df(16)A*$^{+/-}$ mice; ANOVA two-way RM results for genotype were as follows: F(1,4) = 0.001, p = 0.97; results for stimulation were as follows: F(2.1,8.5) = 40.9, p = 3.85 × 10^{-5}; and results for genotype × stimulation were as follows: F(1.2,4.6) = 0.062, p = 0.84 for the PSP before GABA receptor blockers; ANOVA two-way RM results for genotype were as follows: F(1,4) = 0.002, p = 0.97; results for stimulation were as follows: F(2.0,8.2) = 77.22, p = 4.5 × 10^{-6}; and results for genotype × stimulation were as follows: F(1.2,4.9) = 0.053, p = 0.87 after GABA receptor blockers) and no difference in the amplitude of the deduced IPSP (Figure 3F; ANOVA two-way RM results for genotype were as follows: F(1,3) = 0.42, p = 0.56; results for stimulation were as follows: F(2.2,6.7) = 26.3, p = 5.8 × 10^{-4}; and results for genotype × stimulation were as follows: F(1.9,5.9) = 0.32, p = 0.73). These results indicate that the change in inhibitory transmission in *Df(16)A*$^{+/-}$ mice is input specific, with a decrease in feedforward inhibition recruited by SC proximal inputs but no change in feedforward inhibition recruited by distal inputs.

Adult *Df(16)A*$^{+/-}$ Mice CA2 Pyramidal Neurons Have a More Hyperpolarized Resting Membrane Potential

A large feedforward inhibition prevents CA3 SC inputs from evoking action potential firing in CA2 PNs. However, when inhibition is pharmacologically blocked, stimulation of SC inputs can easily evoke action potential firing in CA2 PNs. Because feedforward inhibition is reduced in *Df(16)A*$^{+/-}$ mice, SC stimulation should more easily evoke action potential firing in these mice. However, this only holds true if other parameters such as the intrinsic properties of CA2 PNs are identical in *Df(16)A*$^{+/-}$ mice. Therefore, we measured intrinsic properties of pyramidal neurons in CA2, as well as the depolarizing sag observed during a hyperpolarizing pulse and the action potential threshold. We found that mature (≥6 weeks old) but not young *Df(16)A*$^{+/-}$ mice had a more hyperpolarized resting potential (Figure 4A; results at post-natal week 5 were as follows: −76.6 ± 1.22 mV for WT, n = 12; −77.4 ± 0.9 mV for *Df(16)A*$^{+/-}$ mice, n = 9, t test: p = 0.63; results at post-natal week ≥6–7 were as follows: −76.4 ± 0.5 mV for WT, n = 39; −79.8 ± 0.5 mV for *Df(16)A*$^{+/-}$ mice, n = 51; ANOVA two-way results for genotype were as follows: F(1,81) = 20.45, p = 2.06 × 10^{-5}; results for age were as follows: F(3,81) = 0.12, p = 0.94; and results for genotype × age were as follows: F(3,81) = 0.33, p = 0.79). A lower membrane resistance in *Df(16)A*$^{+/-}$ mice was also observed at post-natal week 9–10 (Figure 4B), but this effect was transient and not observed in older animals. The other parameters measured, including membrane capacitance, depolarizing sag, and action potential threshold, were not different between WT and *Df(16)A*$^{+/-}$ mice (Figures 4C–4E). Paralleling the change in synaptic transmission occurring in mature *Df(16)A*$^{+/-}$ mice, the membrane potential of CA2 PNs becomes more hyperpolarized in *Df(16)A*$^{+/-}$ mice over the sixth to seventh week of life.

We next explored the molecular mechanism underlying the change in membrane potential of CA2 PNs in *Df(16)A*$^{+/-}$ mice. Among the channels known to control resting membrane potential, the two-pore-domain potassium channel TREK is a strong candidate because it is highly expressed in area CA2 (Talley

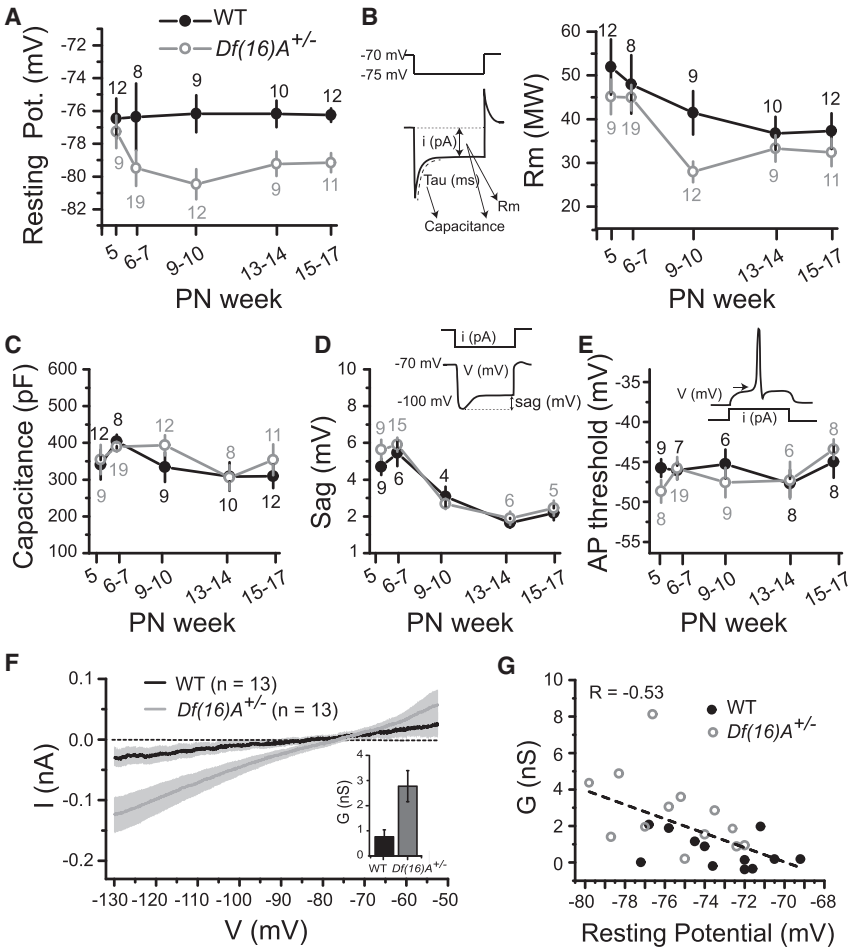

Figure 4. Adult CA2 PNs in *Df(16)A*$^{+/-}$ Mice Have a More Hyperpolarized Resting Potential

Summary graphs and diagrams illustrating how the measurements were made of the resting membrane potential (A), the membrane resistance (Rm) (B), the membrane capacitance (C), the depolarizing sag during a hyperpolarizing current step (D), and the action potential threshold (E) measured in CA2 PNs in WT and in *Df(16)A*$^{+/-}$ mice at different post-natal weeks. The number of cells is shown for each data point. (F) The fluoxetine-sensitive current evoked by a voltage ramp for WT (n = 13) and *Df(16)A*$^{+/-}$ mice (n = 13). Gray shading indicates the SEM. Inset, the estimated conductance of this current, likely due to TREK channels. (G) A plot of the TREK-1 conductance versus resting membrane potential for all of the recorded cells, showing the correlation between the TREK conductance and resting membrane potential (Pearson's $R = -0.53$). Error bars show SEM. See also Figure S3.

et al., 2001) and can be modulated by numerous second messengers (Honoré, 2007). To isolate TREK current, we blocked voltage-activated Ca^{2+}, K^+, Na^+, and HCN channels (with Cd^{2+}, Ni^{2+}, TEA, 4AP, TTX, and Cs^+) and applied a ramp protocol while recording in whole-cell voltage clamp mode before and after application of 100 μM fluoxetine, a potent blocker of TREK channels (Kennard et al., 2005). We restricted the analysis of the ramp between −130 and −50 mV because a large inward current was evoked at more depolarized potentials (Figure S3). We found that the fluoxetine-sensitive current was much larger in *Df(16)A*$^{+/-}$ mice as compared to WT control mice (Figure 4F). We calculated the conductance of the fluoxetine-sensitive current by fitting the slope of the I/V curves and found that it was over three times larger in *Df(16)A*$^{+/-}$ mice (Figure 4F, inset; 0.76 pS, n = 13, 4 mice for WT; 2.77 pS, n = 13, 5 mice for *Df(16)A*$^{+/-}$ mice; t test, p = 0.018). We also observed a significant correlation between the resting membrane potential of the cells and the amount of fluoxetine-sensitive current when the values from WT and *Df(16)A*$^{+/-}$ mice were plotted together (Figure 4G; Pearson's R = −0.53, ANOVA F(1,23) = 9.03, p = 0.006). Together, these data show that the current mediated by TREK channels is upregulated in *Df(16)A*$^{+/-}$ mice and potentially contributes to the more hyperpolarized PN resting potential.

Decreased Action Potential Firing of Pyramidal Neurons in *Df(16)A*$^{+/-}$ Mice in Response to Proximal and Distal Inputs Stimulation

Because of alterations in intrinsic properties, it is difficult to predict which of the changes observed in *Df(16)A*$^{+/-}$ mice, i.e., the decrease in inhibition or the lower resting membrane potential, will have a stronger impact on the ability of CA2 PNs to fire action potentials in response to stimulation of proximal and distal inputs. Therefore, we directly addressed this question by applying a train of 5 pulses at 100 Hz to proximal and distal inputs and quantified the number of action potentials evoked in CA2 PNs in WT and *Df(16)A*$^{+/-}$ mice. With inhibition intact, no action potentials were observed when stimulating proximal inputs, both in WT and *Df(16)A*$^{+/-}$ mice. Only a few cells (2/11) in WT fired action potentials in response to distal input stimulation, indicating that despite the decrease in inhibition, excitatory input does not drive action potential firing more readily in CA2 PNs of *Df(16)A*$^{+/-}$ mice. We then performed the same experiment after blocking inhibition to increase the percentage of cells firing an action potential. In response to SC stimulation, both the number of action potentials during the train and the percentage of cells firing at least one action potential were significantly smaller in *Df(16)A*$^{+/-}$ mice (Figures 5A and 5B; at 30 V stimulation results for WT mice were as follows: 2.23 ± 0.52 AP per train, 83.3% of cell firing, n = 12, 9 mice; results for *Df(16)A*$^{+/-}$ mice were as follows: 0.56 ± 0.38 AP per train, 38.8% of cell firing, n = 18, 11 mice; at 20 and 30V ANOVA two-way RM results for genotype were as follows: F(1,11) = 6.01, p = 0.03; results for stimulation were as follows: F(1.11) = 7.21, p = 0.02; results for genotype × stimulation were as follows: F(1,11) = 0.32, p = 0.58). Because the threshold for action-potential firing was not different between WT and *Df(16)A*$^{+/-}$ mice, this result suggests that the decreased ability to fire action potential results from the more hyperpolarized membrane

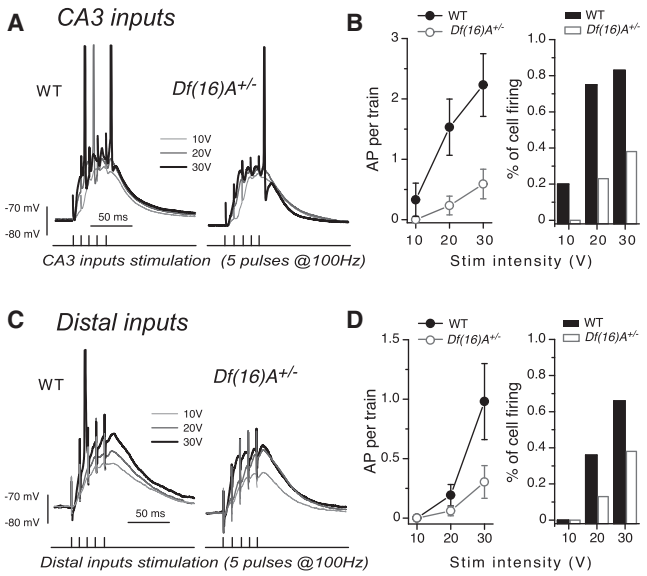

Figure 5. Action Potential Firing of CA2 PNs Is Decreased in Adult *Df(16)A*$^{+/-}$ Mice

(A) Sample traces of the depolarization of CA2 PNs in response to stimulation of SC inputs (5 pulses at 100 Hz) in WT and *Df(16)A*$^{+/-}$ mice.

(B) Summary graph of the number of action potentials (left) and of the percentage of cells firing at least one action potential (right) during the train of stimulation of CA3 inputs at different intensities (10, 20, and 30 V) in WT (n = 12) and *Df(16)A*$^{+/-}$ mice (n = 18).

(C) Sample traces of the depolarization of CA2 PNs in response to a stimulation of distal inputs (5 pulses at 100 Hz) in WT and in *Df(16)A*$^{+/-}$ mice.

(D) Summary graph of the number of action potentials (left) and of the percentage of cells firing at least one action potential (right) during the train of stimulation of distal inputs at different intensities (10, 20, and 30 V) in WT (n = 12) and in *Df(16)A*$^{+/-}$ mice (n = 17). Error bars show SEM. See also Figure S4.

potential of PNs in *Df(16)A*$^{+/-}$ mice. Indeed, the resting potential of PNs in *Df(16)A*$^{+/-}$ mice was more hyperpolarized even after blocking inhibitory transmission (Figure S4A; results for WT mice were as follows: −73.3 ± 0.5 mV, n = 13, 8 mice; results for *Df(16)A*$^{+/-}$ mice were as follows: −75.4 ± 0.7 mV, n = 15, 9 mice; t test, p = 0.04), and injection of a small depolarizing current in PNs of *Df(16)A*$^{+/-}$ mice to compensate for the more hyperpolarized resting potential was sufficient to restore the number of action potentials to a level similar to WT mice (Figure S4B; results at 30 V stimulation were as follows: 0.66 ± 0.55 action potentials per train at resting membrane potential; 2.21 ± 0.73 AP per train after depolarization; n = 9, 7 mice; ANOVA two-way RM results for depolarization were as follows: F(1,8) = 11.1, p = 0.01; results for stimulation were as follows: F(1.2,10.2) = 12.1, p = 0.004; and results for depolarization × stimulation were as follows: F(1.1,9.2) = 12.4, p = 0.005; ANOVA two-way RM results for genotype were as follows: F(1,7) = 5.9 × 10^{-4}, p = 0.0.98; results for stimulation were as follows: F(1.4,10.0) = 21.4, p = 4.6 × 10^{-4}; and results for genotype × stimulation were as follows: F(1.2,8.3) = 0.17, p = 0.73 between WT and *Df(16)A*$^{+/-}$ mice after depolarization). We then looked at action potential firing in response to stimulation of distal inputs. Again, both the number of action potentials per train and the percentage of cells firing at least one action potential were reduced in *Df(16)A*$^{+/-}$ mice (Figures 5C and 5D; results at 30 V stimulation for WT mice were as follows: 0.98 ± 0.32 AP per train, 66.6% of cell firing, n = 12, 9 mice; results for *Df(16)A*$^{+/-}$ mice were as follows: 0.30 ± 0.13 AP per train, 38.8% of cell firing, n = 17, 9 mice; results at 30 V for ANOVA one-way were as follows: F(1,27) = 4.6, p = 0.04). These results show that the decrease in feedforward inhibition did not facilitate action potential firing in response to proximal- and distal-input stimulation. Instead, the more hyperpolarized resting potential of CA2 PNs resulted in a nonspecific decrease in action potential firing, affecting the excitatory drive of both proximal and distal inputs.

Plasticity at Inhibitory Synapses and the Resulting Disinhibitory Increase in SC-CA2 Synaptic Drive Are Impaired in *Df(16)A*$^{+/-}$ Mice

While it is well-established that CA2 PNs cannot undergo a postsynaptic LTP (Zhao et al., 2007), the inhibitory transmission from PV+ INs in this region expresses a long-term depression (iLTD) dependent on delta opioid receptor activation (Piskorowski and Chevaleyre, 2013). Because the density of PV+ INs and inhibitory transmission are reduced in *Df(16)A*$^{+/-}$ mice, we first asked whether the magnitude of iLTD might also be reduced in these mice. For this, we directly monitored inhibitory transmission in CA2 PNs in the presence of AMPA/NMDA receptor blockers (NBQX, D-APV). After collecting a stable baseline, we provided a high-frequency stimulation (HFS; two trains of 100 pulses at 100 Hz). As shown in Figure 6A, this protocol led to a robust and lasting depression of IPSCs in WT mice (63.4% ± 3.0% of baseline, n = 9, 5 mice). Consistent with a presynaptic locus of expression, iLTD resulted in a significant increase in the PPR (Figure 6B; 116.6% ± 5.6%, from 0.47 ± 0.02 to 0.55 ± 0.03; paired t test, p = 0.001). Although the same stimulation also led to a lasting depression in *Df(16)A*$^{+/-}$ mice, the magnitude of the iLTD (Figure 6A; 83.3% ± 3.1% of baseline, n = 9, 5 mice, p = 0.0003 compared to WT) and the change in PPR (109.7% ± 3.8%, from 0.47 ± 0.03 to 0.51 ± 0.03, paired t test, p = 0.03) were strongly reduced in these mice. These results show that plasticity at inhibitory synapses in area CA2 is impaired in *Df(16)A*$^{+/-}$ mice, likely because the subpopulation of inhibitory neurons that express iLTD, i.e., PV+ INs, is also reduced in *Df(16)A*$^{+/-}$ mice.

The iLTD in area CA2 allows for an increase in the net excitatory drive of SC inputs onto CA2 PNs (Nasrallah et al., 2015), resulting in an increased PSP amplitude following iLTD induction. Because iLTD is reduced in *Df(16)A*$^{+/-}$ mice, we wondered whether the disinhibitory-mediated increase in PSP might also be impaired. In order to test this, we performed whole-cell current-clamp recordings and injected current as necessary to maintain the same resting membrane potential for WT and *Df(16)A*$^{+/-}$ mice. Under these conditions, we found a much smaller increase in the PSP amplitude following HFS in *Df(16)A*$^{+/-}$ mice (Figure 7A; results for WT were as follows: 236.1% ± 10.1%, n = 6, 4 mice; results for *Df(16)A*$^{+/-}$ mice were as follows: 137.6% ± 4.5%, n = 8, 6 mice; p < 0.00001 with WT). As previously reported, we verified that this increase in PSP was mediated by a disinhibition as it was abolished in presence of GABA receptor blockers, both in WT and *Df(16)A*$^{+/-}$ mice (Figure 7A; results for WT were as follows: 105.9% ± 7.9%, n = 4,

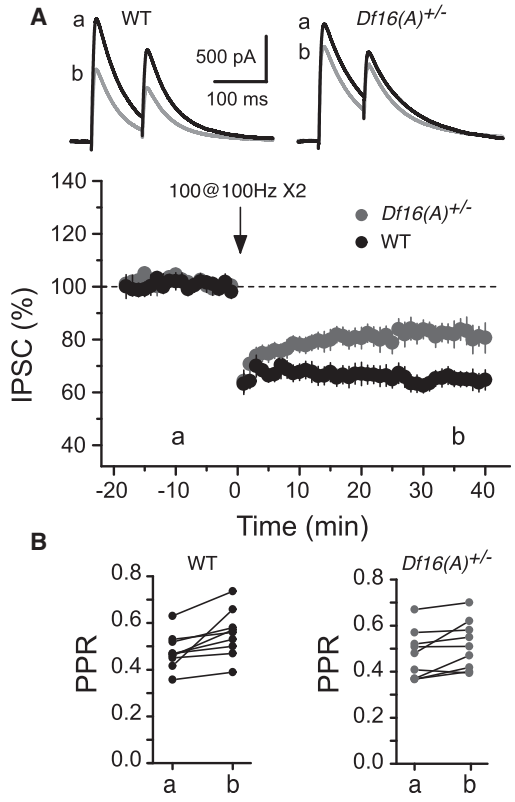

Figure 6. Long-Term Depression at Inhibitory Transmission onto CA2 PNs Is Decreased in Adult *Df(16)A*$^{+/-}$ Mice

(A) Summary graph of normalized IPSCs recorded before and after delivery of tetanic stimulation (100 pulses at 100 Hz twice) in WT (n = 9) and *Df(16)A*$^{+/-}$ mice (n = 9). Sample traces corresponding to the time points before (a) and after (b) tetanus are shown on top.

(B) The paired-pulse ratio for individual experiments before (a) and after (b) tetanic stimulation for WT and *Df(16)A*$^{+/-}$ mice. Error bars show SEM.

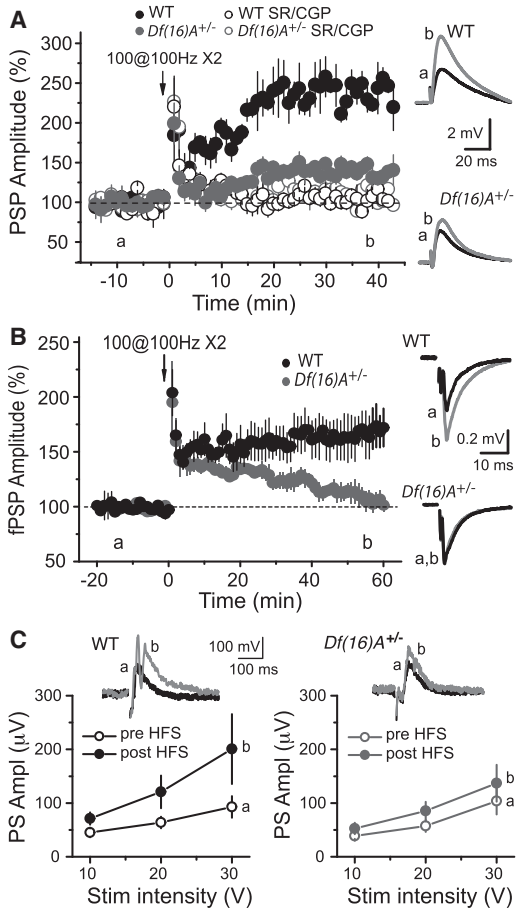

Figure 7. The Disinhibitory Increase in PSP Amplitude and in Action Potential Firing Is Impaired in Adult *Df(16)A*$^{+/-}$ Mice

(A) Summary graph of the change in the amplitude of the PSP recorded in whole-cell current-clamp configuration in response to SC input stimulation following a high-frequency stimulation (100 pulses at 100 Hz repeated twice). The lasting increase in the depolarizing component of the PSP in WT mice (black-filled circles, n = 6) is significantly smaller in *Df(16)A*$^{+/-}$ mice (gray-filled circles, n = 8). This increase is dependent on inhibitory transmission and is blocked by GABA receptor blockers (SR/CGP) both in WT (black open circles, n = 4) and in *Df(16)A*$^{+/-}$ mice (gray open circles, n = 5). Cells were held at −70 mV.

(B) Summary graph of the change in the amplitude of the field PSP recorded extracellularly in response to CA3 input stimulation following a high-frequency stimulation (HFS: 100 pulses at 100 Hz repeated twice) in WT (black, n = 6) and in *Df(16)A*$^{+/-}$ mice (gray, n = 5).

(C) Summary graphs of the amplitude of the population spike monitored extracellularly in the somatic layer of area CA2 in response to SC input stimulation before (a) and after (b) HFS in WT (left, n = 14) and in *Df(16)A*$^{+/-}$ mice (right, n = 14). Error bars show SEM.

4 mice; results for *Df(16)A*$^{+/-}$ mice were as follows: 111.0% ± 2.4%, n = 5, 5 mice; p = 0.52 with WT).

Because CA2 PNs are more hyperpolarized in *Df(16)A*$^{+/-}$ than WT mice, the impact of inhibition on the EPSP might also be reduced due to a smaller driving force for Cl^-. Therefore, in order to test the effect of HFS without affecting the resting membrane potential and Cl^- concentration in the PNs, we performed extracellular recordings to monitor the effect of induction of iLTD by HFS on SC-CA2 field PSP (fPSP) amplitude. We found that the lasting increase in fPSP amplitude was completely abolished in *Df(16)A*$^{+/-}$ mice (Figure 7B; results for WT were as follows: 165.7% ± 20.8%, n = 6, 5 mice; results for *Df(16)A*$^{+/-}$ mice were as follows: 110.2% ± 6.9%, n = 5, 4 mice; p = 0.04 between WT and *Df(16)A*$^{+/-}$ mice). Therefore, these data suggest that the more profound impairment in the disinhibitory-mediated plasticity observed using extracellular recordings results from both the reduced plasticity of inhibitory transmission and the more hyperpolarized resting potential of pyramidal cells in *Df(16)A*$^{+/-}$ mice.

Under basal conditions, area CA2 PNs are primarily inhibited by SC input stimulation. However, following the induction of iLTD in area CA2, stimulation of SC inputs is able to drive action potential firing in CA2 PNs (Nasrallah et al., 2015). To address whether action potential firing is impaired after induction of plasticity in *Df(16)A*$^{+/-}$ mice, we monitored action potential firing extracellularly in the somatic layer of area CA2 before and after HFS. In the majority of experiments in both WT and *Df(16)A*$^{+/-}$ mice (20/28 slices), there was no detection of action potential firing before HFS, which would be observed in

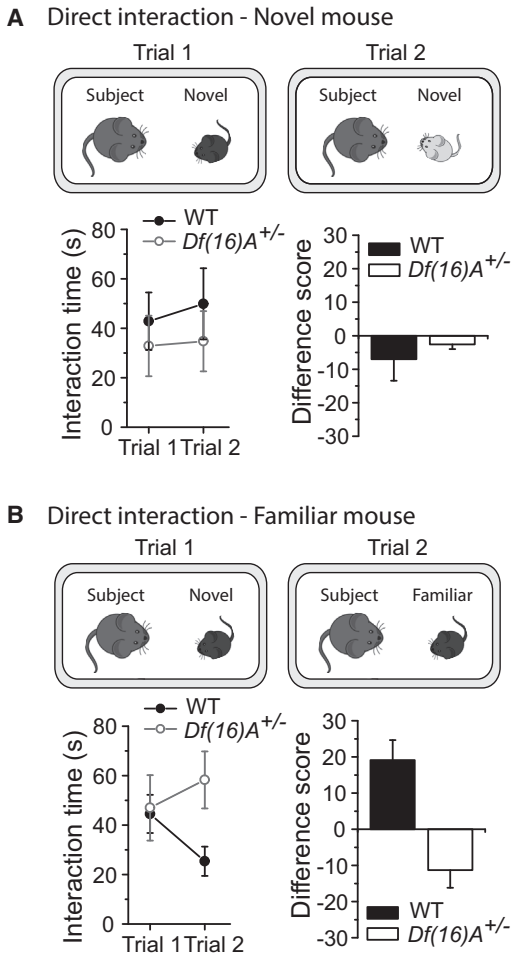

Figure 8. Social Memory Is Impaired in Adult *Df(16)A*$^{+/-}$ Mice

(A) Top: experimental setup for the direct interaction test in which a different stimulus animal was presented in trials 1 and 2. Bottom left: the two groups (*Df(16)A*$^{+/-}$, n = 8; WT, n = 8) engaged in social interaction with the two stimulus animals for a similar amount of time. Bottom right: *Df(16)A*$^{+/-}$ mice and their WT littermates have similar difference scores when interacting with two novel juvenile mice (one-way ANOVA, F(1,15) = 0.469, p = 0.504).

(B) Top: experimental setup for the direct interaction test in which the same stimulus animal was presented for both trials 1 and 2. Bottom left: unlike WT, *Df(16)A*$^{+/-}$ mice fail to show significant recognition of the familiar animal (two-way RM ANOVA for genotype × trial, F(1,14) = 13.503, p = 0.0025). Social memory in the WT mice is evidenced by a decrement in social investigation on trial 2, which is not the case for the *Df(16)A*$^{+/-}$ mice. Bottom right: the difference score of the *Df(16)A*$^{+/-}$ group was not only less than that of the WT group but even had a negative value, indicating that the *Df(16)A*$^{+/-}$ show no social memory when tested with this paradigm. Error bars show SEM.

the extracellular recording configuration as a population spike (PS) (Figure 8C). This confirms that most CA2 PNs are not firing action potentials in response to SC stimulation in basal conditions. Following an HFS, a large PS was observed in WT mice in response to SC stimulation (Figure 7C, left; for instance, from 92.8 ± 19.9 to 200.6 ± 64.8 μV at 30 V stimulation; ANOVA two-way RM results for HFS were as follows: F(1,13) = 5.8, p = 0.03; results for stimulation were as follows: F(1.0,13.7) = 4.65, p = 0.04; and results for HFS × stimulation were as follows: F(1.0,13.7) = 2.7, p = 0.11, n = 14, 4 mice). In *Df(16)A*$^{+/-}$ mice, HFS did not reveal a PS even at the highest stimulation setting (Figure 7C, right; for instance, from 103.7 ± 24.8 to 136.9 ± 34.2 μV at 30 V stimulation; ANOVA two-way RM for HFS were as follows: F(1,13) = 2.9, p = 0.11; results for stimulation were as follows: F(1.1,14.6) = 9.7, p = 0.005; and results for HFS × stimulation were as follows: F(1.1,14.3) = 0.65, p = 0.44, n = 14, 4 mice). These results show that the activity-dependent ability of CA3 PNs to engage CA2 PNs is strongly impaired in *Df(16)A*$^{+/-}$ mice.

Social Memory Is Impaired in *Df(16)A*$^{+/-}$ Mice

Social dysfunction is a hallmark of several psychiatric diseases. Interestingly, it was recently shown that targeted genetic silencing of CA2 PNs results in a strong deficit in social memory formation (Hitti and Siegelbaum, 2014). Because our results show that AP firing in CA2 PNs is strongly reduced in *Df(16)A*$^{+/-}$ mice, both under basal conditions and following activity-dependent plasticity at inhibitory synapses, we wondered if this reduced level of CA2 PN activity would have a similar effect on social learning as the complete silencing of CA2 PNs.

In order to test this hypothesis, we used the direct interaction test. For this test, a subject mouse is first exposed to an unfamiliar mouse during trial 1. During trial 2, the subject mouse is either exposed to a second novel mouse (Figure 8A) or re-exposed to the same mouse encountered in trial 1 (Figure 8B). We found that exploration time for trials 1 and 2, when the subject mouse encountered two different novel mice, was similar in WT and *Df(16)A*$^{+/-}$ mice (ANOVA two-way RM results for genotype × trial were as follows: F(1,14) = 0.602, p = 0.451; results for genotype were as follows: F(1,14) = 0.510, p = 0.487; and results for trial were as follows: F(1,14) = 1.806, p = 0.200). As a result, the difference score (difference in time that the subject mouse spends exploring the other mouse between trials 1 and 2) was also similar between WT and *Df(16)A*$^{+/-}$ mice (Figure 8A; −7.0 ± 6.4, n = 8 for WT and −2.6 ± 1.4, n = 8 for *Df(16)A*$^{+/-}$ mice; results for one-way ANOVA were as follows: F(1,15) = 0.469, p = 0.5). This result suggests that sociability is not impaired in *Df(16)A*$^{+/-}$ mice.

We then tested whether social memory was affected in *Df(16)A*$^{+/-}$ mice. As previously reported, when the subject mouse was re-exposed to the same mouse encountered in trial 1, the interaction time for trial 2 was strongly decreased in WT mice (Figure 8B; from 44.5 s to 25.3 s, $p < 0.01$, Bonferroni post test, n = 8), leading to a difference score of 19.1 ± 5.5. However, social memory was strongly impaired in *Df(16)A*$^{+/-}$ mice. Indeed, unlike WT mice, *Df(16)A*$^{+/-}$ mice did not spend less time exploring a previously encountered mouse (from 47.0 s to 58.3 s, $p > 0.05$, Bonferroni post test, n = 8) and failed to show significant recognition of the familiar mouse (results for two-way RM ANOVA for genotype × trial were as follows: F(1,14) = 13.503, p = 0.0025; results for WT were as follows: $p < 0.01$; results for *Df(16)A*$^{+/-}$ were as follows: $p > 0.05$ Bonferroni post-tests; results for trial were as follows: F(1,14) = 1.998, p = 0.79; and results for genotype were as follows: F(1,14) = 1.236, p = 0.285). The difference score was not only lower than that of WT mice (−11.3 ± 4.9, one-way ANOVA,

p = 0.002) but also had a negative value, indicating no social learning of the *Df(16)A*$^{+/-}$ mice with this test.

These results indicate that social learning, but not sociability, is impaired in *Df(16)A*$^{+/-}$ mice, hence mimicking the phenotype observed in mice with complete CA2 PN silencing. Thus, our data provide a potential cellular mechanism for the impairment in social memory observed in patients with schizophrenia.

DISCUSSION

In this study, we reveal cellular alterations in the 22q11.2 mouse model of schizophrenia that occur uniquely in area CA2 of the hippocampus, and we highlight social memory impairment in these mice, a behavior critically dependent on area CA2. In detail, we have shown that the density of PV+ INs is reduced in area CA2 of *Df(16)A*$^{+/-}$ mice and that the level of feedforward inhibitory transmission onto CA2 PNs is also reduced. In addition, similar to the disease onset in early adulthood in humans, these differences were not present in 4-week-old mice. We also found age-dependent changes in the intrinsic properties of CA2 PNs in *Df(16)A*$^{+/-}$ mice, causing the cells to be more hyperpolarized. As a consequence, CA2 PNs in *Df(16)A*$^{+/-}$ mice displayed fewer action potentials in response to both proximal and distal excitatory input stimulation. Furthermore, the unique plasticity of inhibitory synapses in area CA2 that typically undergoes an activity-dependent iLTD is reduced in *Df(16)A*$^{+/-}$ mice, disrupting the disinhibitory mechanism that allows CA3 to drive action potential firing in CA2 PNs. Thus, information transfer and activity-dependent modulation of the excitatory drive between CA3 and CA2 are strongly impaired in *Df(16)A*$^{+/-}$ mice. Finally, *Df(16)A*$^{+/-}$ mice display a deficit in social memory, a phenotype similar to the one observed after complete silencing of CA2 PNs (Hitti and Siegelbaum, 2014).

Loss of PV+ INs: Significance, Consequences, and Potential Causes

Consistent with our findings, a decrease in PV+ IN density uniquely in area CA2 has been observed both in human postmortem studies and pharmacological animal models (Benes et al., 1998; Berretta et al., 2009; Knable et al., 2004; Zhang and Reynolds, 2002), recapitulating one of the most consistent changes observed in the hippocampus during schizophrenia. A decrease in PV+ IN number in area CA2 has also been reported in bipolar disorder (Benes et al., 1998) and in Alzheimer's disease-affected brains (Brady and Mufson, 1997).

The overall importance of PV+ INs is quite clear: global impairment of PV+ IN function has been shown to disrupt hippocampal network synchrony and was accompanied by profound changes in working and spatial memory (Fuchs et al., 2007; Korotkova et al., 2010). Furthermore, it has recently been shown that hippocampal PV+ basket cells play a pivotal role in regulating memory formation in an experience-dependent manner (Donato et al., 2013). However, previous investigations of hippocampal properties and plasticity of *Df(16)A*$^{+/-}$ mice have revealed only fairly modest changes in inhibitory transmission and plasticity at the SC-CA1 synapse (Drew et al., 2011; Earls et al., 2010). Furthermore, an examination of the theta oscillation and hippocampal synchrony of the *Df(16)A*$^{+/-}$ mice found no difference with control animals (Sigurdsson et al., 2010).

The major aim of this study was to test the hypothesis that the PV+ INs in area CA2 in *Df(16)A*$^{+/-}$ mice are reduced and to examine the resulting consequences in the local network. It has recently been shown that the density of PV+ INs in mice is much higher in area CA2 compared to CA1 and CA3 (Botcher et al., 2014; Piskorowski and Chevaleyre, 2013), and the age-dependent reduction of PV+ staining uniquely in area CA2 of the hippocampus that we observe suggests that inhibitory transmission from PV+ cells in this region may be playing a peculiar function. These INs undergo a unique long-lasting delta opioid-mediated plasticity (Piskorowski and Chevaleyre, 2013) that allows the otherwise nonplastic CA2 PNs (Zhao et al., 2007) to be incorporated into the hippocampal trisynaptic circuit (Nasrallah et al., 2015).

The most predictable consequence of the reduction in CA2 PV+ staining is the reduction in feedforward inhibition between CA3 and CA2 PNs. It is difficult to establish a quantitative link between the decrease in PV+ IN density, the decrease in inhibitory transmission, and the decrease in plasticity, due to uncertainty in the subclass of PV+ cells that are affected and in the effect that PV+ cell reduction has in iLTD and controlling the PSP amplitude. Nevertheless, the ~35% decrease in PV+ INs can account for the ~30% decrease in inhibitory transmission, and the resulting increase in EPSP amplitude (by ~60%) can account for the decrease in disinhibitory LTP (due to an occlusion effect). Furthermore, we have shown that PV+ INs undergo iLTD (Piskorowski and Chevaleyre, 2013) and that the disinhibitory increase in PSP is entirely mediated through a decrease in inhibition resulting from iLTD (Nasrallah et al., 2015). Therefore, although it is difficult to make a quantitative link, we believe that the change in PV+ cell density, the change in IPSP and EPSP amplitude, and the change in plasticity are causally linked. A potential additional outcome of the loss of inhibition is the parallel age-dependent change in intrinsic properties of CA2 PNs. Although an exhaustive study would be required to carefully examine the precise time course of the change in inhibitory transmission, we postulate that the more hyperpolarized membrane potential of CA2 PNs is a compensatory effect of the decrease in inhibition. Indeed, a persistent decrease in inhibitory transmission in CA2 might have a damaging effect on the homeostasis of the hippocampus, as several studies have reported a decrease or loss of inhibition in CA2 during epilepsy (Andrioli et al., 2007; Cohen-Gadol et al., 2004; Olney et al., 1983), and it has been shown that epileptic bursts in human hippocampus are generated in area CA2 (Wittner et al., 2009).

Interestingly, similar to findings that have revealed disinhibition dysfunction in the neocortex (O'Donnell, 2011), our results indicate that periadolescent changes in hippocampal disinhibitory networks are also disrupted. The cause of the loss of PV staining and feedforward inhibition after 4 weeks is an intriguing and pertinent question given the parallel nature of disease onset in humans.

Area CA2 and Neuropsychiatric Disorders

Our analysis of a mouse model of the 22q11.2DS revealed that CA2 PNs are essentially rendered silent due to changes in their

inherent properties, and the loss of inhibitory transmission prevents activity-dependent plasticity from increasing excitatory drive onto these cells. This finding potentially holds great significance when one considers the *output* of area CA2. It has been shown recently that CA2 PNs project to several extrahippocampal structures such as the medial entorhinal cortex (Rowland et al., 2013), the medial and lateral septum, the diagonal band of broca, and the hypothalamic supramammillary nucleus (Cui et al., 2013). Thus, if one also considers the diverse and numerous *inputs* of area CA2, which include but are not limited to cortical, hypothalamic, and intrahippocampal origins (Chevaleyre and Siegelbaum, 2010; Cui et al., 2013; Hitti and Siegelbaum, 2014; Kohara et al., 2014), CA2 is poised to be a hub connecting the hippocampus with multiple brain regions. Previously, it has been reported that the *Df(16)A*$^{+/-}$ mice have reduced performance during a working-memory task and reduced synchrony between the hippocampus and prefrontal cortex (Sigurdsson et al., 2010; Stark et al., 2008) in the absence of any changes in oscillations in the neocortex or hippocampus. While there are multiple ways in which long-range connections can be disrupted, we speculate that the significant changes we see in CA2 PN output may potentially play a role in altering the long-range communication between the hippocampus and numerous other brain regions in the *Df(16)A*$^{+/-}$ mice.

The interesting role of area CA2 in social learning and hippocampal function has only recently emerged. Recent studies have shown that CA2 is essential for social memory (Hitti and Siegelbaum, 2014; Stevenson and Caldwell, 2014). In addition, vasopressin 1b receptor, which is selectively expressed in CA2 PNs, has been shown to be a key player in modulating social memory and aggression in rodents (Stevenson and Caldwell, 2012; Young et al., 2006). In fact, rescue of vasopressin 1b receptor expression specifically in area of CA2 in the hippocampus restored socially motivated attack responses in vasopressin 1b receptor knockout mice (Pagani et al., 2015). Thus, it seems that mice with compromised CA2 function are unable to appropriately assess social situations.

Is there a broader role for area CA2? Recent reports investigating place-cell dynamics indicate this region likely does not encode spatial information but rather displays marked instability over time in the same environment (Lee et al., 2015; Lu et al., 2015; Mankin et al., 2015). A study using immediate-early gene expression revealed that area CA2 is more sensitive than areas CA1 and CA3 to changes in context and may be set to detect conflicts between memory and experience (Wintzer et al., 2014). Remarkably, area CA2 is altered in a number of psychiatric disorders, including schizophrenia and bipolar disorder, as well as in neurodegenerative diseases (Jones and McHugh, 2011). CA2 is connected to subcortical structures, including amygdala, raphe nucleus, and hypothalamic nuclei, and projects to higher cortical structures. Bridging primitive and higher-level structures, the integrity of area CA2 might be necessary to finely tune the interplay between primitive drives (i.e., hypothalamic signals) and higher-level cognition. Thus, we speculate that a compromised area CA2 will result in cognitive dysfunction. Indeed, the level of dementia during Parkinson's disease is associated with the extent of alpha synuclein and of amyloid beta peptide in area CA2 (Kalaitzakis et al., 2009), and the degree of cognitive impairment is correlated with the density of Lewy neurites in area CA2 (Churchyard and Lees, 1997).

Disruption in social cognition is a core symptom of schizophrenia, autism spectrum disorder, and neurodegenerative diseases. In schizophrenia it is among the earlier onset features and is highly correlated with poor functional outcome (Brüne, 2005; Penn et al., 2008). The reciprocal relation of social cognition to both positive (paranoia and delusions) and negative (social withdrawal and reduced motivation) symptoms (Foussias et al., 2014), place it central in current translational strategies (Millan and Bales, 2013). Associations of social cognition impairments with executive function and negative symptoms are particularly evident in the 22q11.2DS (Campbell et al., 2015).

Obviously, rodents do not display all features of human social cognition, and comparable information on cross-species circuit recruitment in social interactions is scarce. What dimensions of altered social cognition are measurable in experimental animal models remain unknown, but there is a need for identification of common neural substrates engaged in animals and humans to facilitate adoption of comparable procedures and common readouts in drug evaluation. In that respect, our results, taken together with previous postmortem studies in patients, suggest that altered circuitry functionality within the CA2 hippocampal area, and its possible interactions with other relevant brain areas, such as the amygdala, from which it receives abundant projections (Pikkarainen et al., 1999), might underlie parts of the social cognition deficits seen in some psychiatric and neurodevelopmental disorders. This region of the hippocampus is consistently overlooked or merged with other CA areas in human imaging studies (Small et al., 2011). Clearly, our results provide strong evidence that this region of the brain merits further study both in animal models of psychiatric diseases and in humans. Furthermore, given the unusual property of neurons in area CA2 to be modulated by numerous neuropeptides (Pagani et al., 2015; Piskorowski and Chevaleyre, 2013; Simons et al., 2012), our results suggest that this pharmacologically unexplored region may be a fruitful therapeutic target for psychiatric diseases.

EXPERIMENTAL PROCEDURES

All animal procedures were performed in accordance with the regulations of the animal care committee of the Université Paris Descartes and of Columbia University.

Slice Preparation

A 400 μm transverse hippocampal slices were prepared from 6- to 17-week-old C57BL6 or *Df(16)A*$^{+/-}$ male mice. Animals were euthanized in accordance with institutional regulations under anesthesia with isofluorane. Hippocampi were removed and placed upright into an agar mold and cut with a vibratome in ice-cold extracellular slicing solution (for solution compositions, see Supplemental Experimental Procedures) The slices were then transferred to 30°C artificial cerebral spinal fluid, ACSF, for 30 min and kept at room temperature for at least 1.5 hr before recording. All experiments were performed at 33°C.

Electrophysiological Recordings and Analysis

Field recordings of PSPs were performed in current-clamp mode with a recording patch pipette (3–5 MΩ) containing 1 M of NaCl and positioned in the middle of *stratum radiatum* of CA2. Whole-cell recordings were obtained from CA2 PNs in current-clamp mode held at −73 mV with a patch pipette (3–5 MΩ) containing a KMethylSulfate-based solution. Inhibitory currents

were recorded with pipette solution containing CesiumMethylSulfate. The liquid junction potential was ~2 mV, and membrane potentials were corrected for this junction potential. Series resistance (typically 12–18 MΩ) was monitored throughout each experiment, and cells with more than 15% change were excluded from analysis. The K^+ current mediated by TREK channels was recorded with a modified ACSF containing reduced sodium and blockers for voltage-gated Ca^{2+}, K^+, Na^+, and cationic channels. Cell-capacity current and access resistance were compensated with the amplifier circuitry, and series resistance compensation was set at 80%–95% and frequently checked during the experiment. We performed a ramp from −120 to +20 mV (liquid junction potential was measured and corrected post hoc) before and after application of fluoxetine to block TREK channels (Figure S3). The subtracted current is shown in Figure 4F; the I/V curves and the conductance was estimated between −130 and −90 mV.

We identified the CA2 PNs by somatic location and size. The cell type was confirmed by several electrophysiological properties (input resistance, membrane capacitance, resting membrane potential, sag amplitude, action potential amplitude, and duration) as previously described (Chevaleyre and Siegelbaum, 2010).

Synaptic potentials were evoked by monopolar stimulation with a patch pipette filled with ACSF and positioned in the middle of CA1 SR. The amplitudes of the PSPs or PSCs were normalized to the baseline amplitude. An HFS (100 pulses at 100 Hz repeated twice) was applied following stable baseline. The magnitude of plasticity was estimated by comparing averaged responses at 30–40 min for whole cell and at 50–60 min for extracellular recordings after the induction protocol with baseline-averaged responses from 0 to 10 min before the induction protocol. We used pClamp10 and Axograph X software for data acquisition and Origin Pro for data analysis. Statistical comparisons were performed using Student's t test or two-way ANOVA with repeated measure (RM), and we used a Greenhouse-Geiser for correction of degrees of freedom when sphericity was not assumed. Results are reported as mean ± SEM.

Immunohistochemistry

For histology experiments, 4- or 8-week-old male mice were transcardially perfused, the brains were dissected and postfixed, and 30 μm floating coronal sections were prepared. Eight serial sections were selected spanning bregma −1.8 to −2.1. A rabbit anti-parvalbumin antibody (Swant) was used at a dilution of 1:2,000; the mouse monoclonal anti-RGS14 antibody (Neuromab) was used at dilution of 1:300. Images were collected with a Zeiss 710 laser-scanning confocal microscope. z series images consisting of two channels were collected every 5 μm over a total distance of 35 μm per slice. RGS14 staining was used to define area CA2. All image analysis was performed with ImageJ.

All experimenters were blind to the genotype of the animals for all recordings, imaging, and analysis (including quantification of PV+ IN density).

Social Memory-Direct Interaction with Juveniles

All mice were housed two to five in each cage and given ad libitum access to food and water. They were kept on a 12 hr (6:00–18:00) light–dark cycle with the room temperature regulated between 21°C and 23°C. Behavioral tests were performed during the light cycle in a testing room adjunct to the mouse housing room, which minimizes any transportation stress. Immediately prior to the experimental sessions, 10- to 12-week-old *Df(16)A*$^{+/-}$ and WT littermates were transferred to the testing room and placed into individual cages, identical to the ones used for housing, where they were allowed to habituate to the new environment for 15 min. Male juvenile mice (C57BL/6J, 4–5 weeks old) were also placed in the testing room in their home cages and allowed to habituate for a similar amount of time. Testing began when a novel juvenile mouse was introduced to a cage with one of the adult experimental mice. Activity was monitored for 5 min (trial 1) and scored online by a trained observer blind to the genotype of the test mice for social behavior (anogenital and nose-to-nose sniffing, close following, and allogrooming) initiated by the experimental subject, as described by (Hitti and Siegelbaum, 2014). After an intertrial interval of 1 hr, the experimental mice were introduced to either the previously encountered mouse or a novel mouse again for 5 min (trial 2). The time spent in social interaction during trial 1 was subtracted from the social interaction time during trial 2 to obtain the difference score. Statistical significance was assessed by one-way ANOVA, or two-way RM ANOVA where appropriate.

SUPPLEMENTAL INFORMATION

Supplemental Information includes Supplemental Experimental Procedures and four figures and can be found with this article online at http://dx.doi.org/10.1016/j.neuron.2015.11.036.

AUTHOR CONTRIBUTIONS

Conceptualization, R.A.P., V.C., S.A.S., and J.A.G.; Investigation, R.A.P., K.N., and V.C. performed all electrophysiology with S.I.H. contributing to TREK recordings; R.A.P. and J.M. performed immunohistology; R.A.P. and V.C. completed imaging and quantification; A.D. completed behavioral experiments; Formal Analysis, V.C. and A.D.; Visualization, R.A.P. and V.C.; Writing – Original Draft, R.A.P. and V.C.; Writing – Review and Editing, R.A.P., V.C., A.D., and J.A.G.; Funding Acquisition, R.A.P., V.C., S.A.S., and J.A.G.; Resources, R.A.P., V.C., S.A.S., and J.A.G.

ACKNOWLEDGMENTS

We would like to thank Yan Sun and Rachel Waldman for taking care of the mouse colony at Columbia University. This work was supported by the CNRS ATIP-Avenir (V.C.), Agence Nationale de la Recherche ANR-12-BSV4-0021-01 (V.C.), ANR-13-JSV4-0002-01 (R.A.P.), the Ville de Paris (R.A.P.), and NIH R01MH097879 (J.A.G).

Received: May 14, 2015
Revised: September 23, 2015
Accepted: November 18, 2015
Published: January 6, 2016

REFERENCES

Andrioli, A., Alonso-Nanclares, L., Arellano, J.I., and DeFelipe, J. (2007). Quantitative analysis of parvalbumin-immunoreactive cells in the human epileptic hippocampus. Neuroscience *149*, 131–143.

Basu, J., Srinivas, K.V., Cheung, S.K., Taniguchi, H., Huang, Z.J., and Siegelbaum, S.A. (2013). A cortico-hippocampal learning rule shapes inhibitory microcircuit activity to enhance hippocampal information flow. Neuron *79*, 1208–1221.

Benes, F.M., Kwok, E.W., Vincent, S.L., and Todtenkopf, M.S. (1998). A reduction of nonpyramidal cells in sector CA2 of schizophrenics and manic depressives. Biol. Psychiatry *44*, 88–97.

Berretta, S., Gisabella, B., and Benes, F.M. (2009). A rodent model of schizophrenia derived from postmortem studies. Behav. Brain Res. *204*, 363–368.

Botcher, N.A., Falck, J.E., Thomson, A.M., and Mercer, A. (2014). Distribution of interneurons in the CA2 region of the rat hippocampus. Front. Neuroanat. *8*, 104.

Brady, D.R., and Mufson, E.J. (1997). Parvalbumin-immunoreactive neurons in the hippocampal formation of Alzheimer's diseased brain. Neuroscience *80*, 1113–1125.

Brüne, M. (2005). Emotion recognition, 'theory of mind,' and social behavior in schizophrenia. Psychiatry Res. *133*, 135–147.

Campbell, L.E., McCabe, K.L., Melville, J.L., Strutt, P.A., and Schall, U. (2015). Social cognition dysfunction in adolescents with 22q11.2 deletion syndrome (velo-cardio-facial syndrome): relationship with executive functioning and social competence/functioning. J. Intellect. Disabil. Res. *59*, 845–859.

Chevaleyre, V., and Siegelbaum, S.A. (2010). Strong CA2 pyramidal neuron synapses define a powerful disynaptic cortico-hippocampal loop. Neuron *66*, 560–572.

Churchyard, A., and Lees, A.J. (1997). The relationship between dementia and direct involvement of the hippocampus and amygdala in Parkinson's disease. Neurology *49*, 1570–1576.

Cohen-Gadol, A.A., Pan, J.W., Kim, J.H., Spencer, D.D., and Hetherington, H.H. (2004). Mesial temporal lobe epilepsy: a proton magnetic resonance spectroscopy study and a histopathological analysis. J. Neurosurg. *101*, 613–620.

Cui, Z., Gerfen, C.R., and Young, W.S., 3rd (2013). Hypothalamic and other connections with dorsal CA2 area of the mouse hippocampus. J. Comp. Neurol. *521*, 1844–1866.

Donato, F., Rompani, S.B., and Caroni, P. (2013). Parvalbumin-expressing basket-cell network plasticity induced by experience regulates adult learning. Nature *504*, 272–276.

Drew, L.J., Stark, K.L., Fénelon, K., Karayiorgou, M., Macdermott, A.B., and Gogos, J.A. (2011). Evidence for altered hippocampal function in a mouse model of the human 22q11.2 microdeletion. Mol. Cell. Neurosci. *47*, 293–305.

Earls, L.R., Bayazitov, I.T., Fricke, R.G., Berry, R.B., Illingworth, E., Mittleman, G., and Zakharenko, S.S. (2010). Dysregulation of presynaptic calcium and synaptic plasticity in a mouse model of 22q11 deletion syndrome. J. Neurosci. *30*, 15843–15855.

Foussias, G., Agid, O., Fervaha, G., and Remington, G. (2014). Negative symptoms of schizophrenia: clinical features, relevance to real world functioning and specificity versus other CNS disorders. Eur. Neuropsychopharmacol. *24*, 693–709.

Fuchs, E.C., Zivkovic, A.R., Cunningham, M.O., Middleton, S., Lebeau, F.E.N., Bannerman, D.M., Rozov, A., Whittington, M.A., Traub, R.D., Rawlins, J.N.P., and Monyer, H. (2007). Recruitment of parvalbumin-positive interneurons determines hippocampal function and associated behavior. Neuron *53*, 591–604.

Hitti, F.L., and Siegelbaum, S.A. (2014). The hippocampal CA2 region is essential for social memory. Nature *508*, 88–92.

Honoré, E. (2007). The neuronal background K2P channels: focus on TREK1. Nat. Rev. Neurosci. *8*, 251–261.

International Schizophrenia Consortium (2008). Rare chromosomal deletions and duplications increase risk of schizophrenia. Nature *455*, 237–241.

Jones, M.W., and McHugh, T.J. (2011). Updating hippocampal representations: CA2 joins the circuit. Trends Neurosci. *34*, 526–535.

Kalaitzakis, M.E., Christian, L.M., Moran, L.B., Graeber, M.B., Pearce, R.K.B., and Gentleman, S.M. (2009). Dementia and visual hallucinations associated with limbic pathology in Parkinson's disease. Parkinsonism Relat. Disord. *15*, 196–204.

Karayiorgou, M., Morris, M.A., Morrow, B., Shprintzen, R.J., Goldberg, R., Borrow, J., Gos, A., Nestadt, G., Wolyniec, P.S., Lasseter, V.K., et al. (1995). Schizophrenia susceptibility associated with interstitial deletions of chromosome 22q11. Proc. Natl. Acad. Sci. USA *92*, 7612–7616.

Karayiorgou, M., Simon, T.J., and Gogos, J.A. (2010). 22q11.2 microdeletions: linking DNA structural variation to brain dysfunction and schizophrenia. Nat. Rev. Neurosci. *11*, 402–416.

Kennard, L.E., Chumbley, J.R., Ranatunga, K.M., Armstrong, S.J., Veale, E.L., and Mathie, A. (2005). Inhibition of the human two-pore domain potassium channel, TREK-1, by fluoxetine and its metabolite norfluoxetine. Br. J. Pharmacol. *144*, 821–829.

Knable, M.B., Barci, B.M., Webster, M.J., Meador-Woodruff, J., and Torrey, E.F.; Stanley Neuropathology Consortium (2004). Molecular abnormalities of the hippocampus in severe psychiatric illness: postmortem findings from the Stanley Neuropathology Consortium. Mol. Psychiatry *9*, 609–620, 544.

Kohara, K., Pignatelli, M., Rivest, A.J., Jung, H.-Y., Kitamura, T., Suh, J., Frank, D., Kajikawa, K., Mise, N., Obata, Y., et al. (2014). Cell type-specific genetic and optogenetic tools reveal hippocampal CA2 circuits. Nat. Neurosci. *17*, 269–279.

Korotkova, T., Fuchs, E.C., Ponomarenko, A., von Engelhardt, J., and Monyer, H. (2010). NMDA receptor ablation on parvalbumin-positive interneurons impairs hippocampal synchrony, spatial representations, and working memory. Neuron *68*, 557–569.

Lee, S.E., Simons, S.B., Heldt, S.A., Zhao, M., Schroeder, J.P., Vellano, C.P., Cowan, D.P., Ramineni, S., Yates, C.K., Feng, Y., et al. (2010). RGS14 is a natural suppressor of both synaptic plasticity in CA2 neurons and hippocampal-based learning and memory. Proc. Natl. Acad. Sci. USA *107*, 16994–16998.

Lee, H., Wang, C., Deshmukh, S.S., and Knierim, J.J. (2015). Neural population evidence of functional heterogeneity along the CA3 transverse axis: pattern completion versus pattern separation. Neuron *87*, 1093–1105.

Lu, L., Igarashi, K.M., Witter, M.P., Moser, E.I., and Moser, M.-B. (2015). Topography of place maps along the CA3-to-CA2 axis of the hippocampus. Neuron *87*, 1078–1092.

Mankin, E.A., Diehl, G.W., Sparks, F.T., Leutgeb, S., and Leutgeb, J.K. (2015). Hippocampal CA2 activity patterns change over time to a larger extent than between spatial contexts. Neuron *85*, 190–201.

Millan, M.J., and Bales, K.L. (2013). Towards improved animal models for evaluating social cognition and its disruption in schizophrenia: the CNTRICS initiative. Neurosci. Biobehav. Rev. *37* (9 Pt B), 2166–2180.

Narr, K.L., Thompson, P.M., Szeszko, P., Robinson, D., Jang, S., Woods, R.P., Kim, S., Hayashi, K.M., Asunction, D., Toga, A.W., and Bilder, R.M. (2004). Regional specificity of hippocampal volume reductions in first-episode schizophrenia. Neuroimage *21*, 1563–1575.

Nasrallah, K., Piskorowski, R.A., and Chevaleyre, V. (2015). Inhibitory plasticity permits the recruitment of CA2 pyramidal neurons by CA3(1,2,3). eNeuro *2*, ENEURO.0049-15.2015.

O'Donnell, P. (2011). Adolescent onset of cortical disinhibition in schizophrenia: insights from animal models. Schizophr. Bull. *37*, 484–492.

Olney, J.W., deGubareff, T., and Sloviter, R.S. (1983). "Epileptic" brain damage in rats induced by sustained electrical stimulation of the perforant path. II. Ultrastructural analysis of acute hippocampal pathology. Brain Res. Bull. *10*, 699–712.

Pagani, J.H., Zhao, M., Cui, Z., Avram, S.K., Caruana, D.A., Dudek, S.M., and Young, W.S. (2015). Role of the vasopressin 1b receptor in rodent aggressive behavior and synaptic plasticity in hippocampal area CA2. Mol. Psychiatry *20*, 490–499.

Penn, D.L., Sanna, L.J., and Roberts, D.L. (2008). Social cognition in schizophrenia: an overview. Schizophr. Bull. *34*, 408–411.

Pikkarainen, M., Rönkkö, S., Savander, V., Insausti, R., and Pitkänen, A. (1999). Projections from the lateral, basal, and accessory basal nuclei of the amygdala to the hippocampal formation in rat. J. Comp. Neurol. *403*, 229–260.

Piskorowski, R.A., and Chevaleyre, V. (2013). Delta-opioid receptors mediate unique plasticity onto parvalbumin-expressing interneurons in area CA2 of the hippocampus. J. Neurosci. *33*, 14567–14578.

Pouille, F., and Scanziani, M. (2001). Enforcement of temporal fidelity in pyramidal cells by somatic feed-forward inhibition. Science *293*, 1159–1163.

Rowland, D.C., Weible, A.P., Wickersham, I.R., Wu, H., Mayford, M., Witter, M.P., and Kentros, C.G. (2013). Transgenically targeted rabies virus demonstrates a major monosynaptic projection from hippocampal area CA2 to medial entorhinal layer II neurons. J. Neurosci. *33*, 14889–14898.

Sigurdsson, T., Stark, K.L., Karayiorgou, M., Gogos, J.A., and Gordon, J.A. (2010). Impaired hippocampal-prefrontal synchrony in a genetic mouse model of schizophrenia. Nature *464*, 763–767.

Simons, S.B., Caruana, D.A., Zhao, M., and Dudek, S.M. (2012). Caffeine-induced synaptic potentiation in hippocampal CA2 neurons. Nat. Neurosci. *15*, 23–25.

Small, S.A., Schobel, S.A., Buxton, R.B., Witter, M.P., and Barnes, C.A. (2011). A pathophysiological framework of hippocampal dysfunction in ageing and disease. Nat. Rev. Neurosci. *12*, 585–601.

Stark, K.L., Xu, B., Bagchi, A., Lai, W.-S., Liu, H., Hsu, R., Wan, X., Pavlidis, P., Mills, A.A., Karayiorgou, M., and Gogos, J.A. (2008). Altered brain microRNA biogenesis contributes to phenotypic deficits in a 22q11-deletion mouse model. Nat. Genet. *40*, 751–760.

Stevenson, E.L., and Caldwell, H.K. (2012). The vasopressin 1b receptor and the neural regulation of social behavior. Horm. Behav. *61*, 277–282.

Stevenson, E.L., and Caldwell, H.K. (2014). Lesions to the CA2 region of the hippocampus impair social memory in mice. Eur. J. Neurosci. *40*, 3294–3301.

Talley, E.M., Solorzano, G., Lei, Q., Kim, D., and Bayliss, D.A. (2001). Cns distribution of members of the two-pore-domain (KCNK) potassium channel family. J. Neurosci. *21*, 7491–7505.

Wintzer, M.E., Boehringer, R., Polygalov, D., and McHugh, T.J. (2014). The hippocampal CA2 ensemble is sensitive to contextual change. J. Neurosci. *34*, 3056–3066.

Wittner, L., Huberfeld, G., Clémenceau, S., Eross, L., Dezamis, E., Entz, L., Ulbert, I., Baulac, M., Freund, T.F., Maglóczky, Z., and Miles, R. (2009). The epileptic human hippocampal cornu ammonis 2 region generates spontaneous interictal-like activity in vitro. Brain *132*, 3032–3046.

Xu, B., Roos, J.L., Levy, S., van Rensburg, E.J., Gogos, J.A., and Karayiorgou, M. (2008). Strong association of de novo copy number mutations with sporadic schizophrenia. Nat. Genet. *40*, 880–885.

Young, W.S., Li, J., Wersinger, S.R., and Palkovits, M. (2006). The vasopressin 1b receptor is prominent in the hippocampal area CA2 where it is unaffected by restraint stress or adrenalectomy. Neuroscience *143*, 1031–1039.

Zhang, Z.J., and Reynolds, G.P. (2002). A selective decrease in the relative density of parvalbumin-immunoreactive neurons in the hippocampus in schizophrenia. Schizophr. Res. *55*, 1–10.

Zhao, M., Choi, Y.-S., Obrietan, K., and Dudek, S.M. (2007). Synaptic plasticity (and the lack thereof) in hippocampal CA2 neurons. J. Neurosci. *27*, 12025–12032.